


EVALUATION OF SPECIFIC ABSORPTION RATE IN THE FAR-FIELD, NEAR-TO-FAR FIELD AND NEAR-FIELD REGIONS FOR INTEGRATIVE RADIOFREQUENCY EXPOSURE ASSESSMENT

Ilaria Liorni¹, Myles Capstick¹, Luuk van Wel², Joe Wiart³, Wout Joseph⁴, Elisabeth Cardis^{5,6,7},

Mònica Guxens^{5,6,7,8}, Roel Vermeulen^{2,9,10} and Arno Thielens¹⁰ ^{4,*}

¹Foundation for Research on Information Technologies in Society (IT²IS), Zeughausstrasse 43, 8004 Zürich, Zurich, Switzerland

²Institute for Risk Assessment Sciences, Utrecht University, P.O. Box 80178, 3508 TD, Utrecht, the Netherlands

³Chaire C2M LTCl, Telecom ParisTech Université Paris Saclay, 46 Rue Barrault, 75013 Paris, Paris, France

⁴Department of Information Technology, Ghent University/IMEC, Technologiepark-Zwijnaarde 126, 9052 Ghent, Ghent, Belgium

⁵ISGlobal, Carrer del Rosselló, 132, 08036 Barcelona, Barcelona, Spain

⁶Universitat Pompeu Fabra (UPF), Plaça de la Mercè, 10-12, 08002 Barcelona, Barcelona, Spain

⁷CIBER Epidemiología y Salud Pública (CIBERESP), C/ Monforte de Lemos 3-5, 28029 Madrid, Madrid, Spain

⁸Department of Child and Adolescent Psychiatry/Psychology, Erasmus MC, University Medical Centre, Doctor Molewaterplein 40, 3015 GD Rotterdam, Rotterdam, the Netherlands

⁹Julius Center for Health Sciences and Primary Care, University Medical Center Utrecht, Universiteitsweg 100, 3584 CG Utrecht, Utrecht, the Netherlands

¹⁰MRC-PHE Centre for Environment and Health, Department of Epidemiology and Biostatistics, School of Public Health, Imperial College London, Norfolk Place, London W2 1PG, London, UK

*Corresponding author: arno.thielens@ugent.be

Received 26 June 2020; revised 26 August 2020; editorial decision 2 September 2020; accepted 10 September 2020

The specific absorption rate (SAR) induced by wireless radiofrequency (RF) systems depends on different parameters. Previously, SAR was mainly assessed under conditions of a single frequency and technology and for a limited number of localized RF sources. The current and emerging mobile systems involve a wider range of usage scenarios and are frequently used simultaneously, leading to combined exposures for which almost no exposure evaluation exists. The aim and novelty of this study is to close this gap of knowledge by developing new methods to rapidly evaluate the SAR induced by RF systems in such scenarios at frequencies from 50 MHz to 5.5 GHz. To this aim, analytical methods for SAR estimation in several usage scenarios were derived through a large-scale numerical study. These include subject-specific characteristics, properties of the RF systems and provide an estimation of the SAR in the whole body, tissues and organs, and different brain regions.

INTRODUCTION

Human exposure to electromagnetic fields (EMFs) in the radiofrequency (RF) range has substantially increased in recent years due to the employment of EMFs in new technologies for use in personal (e.g. health monitoring, sport performance, communication and gaming), domestic (control of appliances, houses) and buildings (alarm systems, smart meters), commercial and industrial environments (electric surveillance, tagging). Personal exposure to such systems is often quantified using the specific absorption rate (SAR), which is the absorbed RF power averaged over a certain mass or volume.^(1–3) This power can be averaged over the whole body (SAR_{wb})^(1,2) or over a

specific tissue or organ, so-called organ-specific SAR (SAR_{osa})⁽³⁾.

The increasing use of new wireless consumer electronics is being accompanied by an increase in the amount of data consumed, which means that new infrastructures, such as those for fifth generation telecommunication (5G), must be deployed^(4,5). Although no conclusive evidence of long-term adverse health effects due to RF-EMFs has been found^(6,7), public concern has grown due to the increasing number and multitude of RF systems operating simultaneously both in close proximity and far away from people.

Epidemiological studies assessing the impact of RF exposure require methods to estimate the dose

that each user or user group are exposed to in order to assess possible association with various health impacts^(8–10). When the second generation of mobile phones was launched and adopted in the 1990's, the only use scenario of RF-EMFs in the general public was the making and receiving of phone calls with the device held next to the head⁽¹¹⁾. The limited number of RF-EMF exposure scenarios and form factors of the phones resulted in the possibility to estimate instantaneous exposure with limited uncertainty⁽¹²⁾. As mobile phones and telecom networks evolved, the usage scenarios multiplied along with the number and types of mobile devices and RF-EMF exposure estimation entered a new and much more complex reality. In addition, there is also an increase in the number and variety of environmental sources that provide wireless access to the users. In order to be able to provide valuable dosimetric assessments of actual exposures of the public in such exposure conditions, exposure estimates continue to be of importance in studies on potential health impacts⁽¹⁰⁾. Hence the need for integrated approximation formulas to take the emitted power, communication protocol, frequency bands and estimated distance of the emitting device to the person exposed to a dose, even though the plethora of use cases will inherently introduce a wider range of uncertainties. In parallel, there has been more interest in epidemiological studies that investigate RF-EMF exposure of certain organs, tissues or brain regions in the human body^(13–16) in order to investigate potential health effects induced by exposure of those tissues.

Previous studies have attempted to estimate the integrative exposure from far-field and near-field sources in terms of 'dose' (in J/kg) obtained by multiplying the amount of time of exposure by the induced SAR^(5,17,18) combined near-and far-field SAR_{wb} and SAR_{osa} values in several frequency bands. In Plets *et al.*⁽¹⁸⁾, prediction models for whole-body exposure due to indoor base-station antennas and access points operating in downlink mode and to mobile devices operating in uplink mode with indoor wireless networks were developed. Finally, in Varsier *et al.*⁽⁵⁾, an exposure index linked to dose was developed for evaluation of EMF exposure induced by wireless cellular networks—i.e. base stations and access points for personal devices and networks—as a function of usage, posture and traffic. Although these studies demonstrate the power of integrated exposure assessment, they are not general enough to be used for RF-EMF exposure assessment of the general population in a wide range of RF-EMF exposure scenarios.

Therefore, this study aims to provide general analytical methods to evaluate the exposure to new and existing RF systems in a wide range of usage scenarios, including new usages that have not yet been tested. These novel analytical methods were derived

from a large-scale numerical study, in which several computational anatomical phantoms were exposed to several RF systems in different usage scenarios, i.e. far-field, near-to-far field and near-field exposure. For each exposure group, novel approximation formulas have been derived to scale the SAR analyzed through numerical simulations in the different usage scenarios, accounting for variations in source location, frequency, gender, age, body mass and morphology. Additionally, the RF-EMF exposure assessment is extended in order to cover new RF technologies, e.g. body-worn sensors, wireless virtual reality (VR) glasses working up to 5.5 GHz, alongside more conventional RF-EMF sources such as mobile phones, tablets, laptops and consoles. Finally, the RF-EMF exposure assessment will consider exposure of the whole body, separate tissues and organs, and different brain regions.

The results presented in this manuscript are important for epidemiological studies, because the proposed approach permits to provide whole-body, tissue-specific and brain-region-specific estimates of the levels of exposure of the general populations due to multiple RF systems, which allow one to investigate the potential long-term health effects. This manuscript does not investigate potential health effects of exposure to RF-EMFs. However, it presents analytical methods for evaluating accumulated RF dose over time, which in their turn are essential for interpreting epidemiological studies of exposure of the general public to environmental and personally induced RF-EMFs from multiple sources over a period of time. Furthermore, it can also be used to evaluate the impact of potential measures for reducing exposure.

MATERIAL AND METHODS

RF exposure scenarios

In this study, human computational anatomical phantoms of the Virtual Population (ViP)^(2,19) developed by the IT'IS Foundation (Zurich, Switzerland) were exposed to RF-EMF at frequencies from 50 MHz to 5.5 GHz (Tables 1, 2, and S1). These frequencies were chosen because they cover almost all currently used telecommunication bands responsible for significant exposure to humans⁽²⁰⁾ and those that will be used in 5G New Radio (NR) systems⁽²¹⁾. Three different exposure scenarios were selected to represent typical exposure configurations of the general population: (a) far-field exposure; (b) near-to-far field exposure; (c) near-field exposure.

As a general definition, in the far-field region, the spatial distance R between the RF system and the exposed subject is $> \frac{2D^2}{\lambda}$, where D is the size of the antenna and λ is the wavelength⁽²²⁾. In this region, the

Table 1. Overview of anatomical structures and ViP phantoms(*) deployed to estimate induced averaged SAR values in the three different field regions (performed calculations are indicated with ‘x’). For cases where only specific tissues and organs have been considered in the analysis, these are explicitly listed.

	SAR _{wb}	SAR _{osa}	SAR _{ds}	ViP phantoms*
Far-field	x	Whole-brain and brain tissues: gray matter, medulla, midbrain, pons	x	Billie (DOI: 10.13099/VIP11003-03-1), Charlie (DOI: 10.13099/ViP-Charlie-V1.1), Duke (DOI: 10.13099/VIP11001-03-1-1), Ella (DOI: 10.13099/VIP11002-03-1), Nina (DOI: 10.13099/ViP-Nina-V1.1), Thelonious (DOI: 10.13099/VIP11004-03-1) Eartha (DOI: 10.13099/VIP11007-03-1)
Near-to-far field	x	Only whole-brain	—	
Near-field:				
On body	x	All tissues	—	Billie, Ella, Fats (DOI: 10.13099/VIP11014-03-2)
Body-worn sensors	x	All tissues	—	Billie, Duke Louis (DOI: 10.13099/VIP11006-03-1)
Smartwatches	x	All tissues	—	Billie, Duke, Louis
Wireless VR	x	Whole-brain and brain structures	x	Billie, Duke Roberta (DOI: 10.13099/VIP11008-03-1)
Tablet	x	All tissues	x	Billie, Duke, Roberta
Mobile phone at the head [Calderon <i>et al.</i> (24)]	—	Whole-brain, different anatomical structures	x	Billie, Duke Eartha, Louis

*The ViP phantoms can be found for download on <https://itis.swiss/virtual-population/virtual-population/vip3/>

Table 2. RF-bands used for the analysis of far-field exposures.

Service	Frequency range (MHz)
FM radio	87.5–108
DVB-T	470–790
DL-800	791–821
UL-800	832–862
UL-900	880–915
DL-900	925–960
UL-1800	1710–1785
DL-1800	1805–1880
DECT	1880–1900
UL-1900	1920–1980
DL-1900	2110–2170
WiFi 2G	2400–2485
UL-2600	2500–2570
DL-2600	2620–2690
WiMax 3.5	3400–3600
WiFi 5G	5150–5875

RF-EMFs generated by the system can be approximated as a set of plane waves^(1,3). In the near-field region, RF systems are at distances $R < 0.62\sqrt{\frac{D^3}{\lambda}}$ to the exposed subject⁽¹⁸⁾. In this region, the electric and magnetic fields are coupled. Hence, exposure to the RF system needs to be simulated on the basis of the actual structure and position of the source. In between the near-field region and the far-field region, one can find the so-called the near-to-far field region. In this transition region between distances $0.62\sqrt{\frac{D^3}{\lambda}} < R < \frac{2D^2}{\lambda}$, both near-field and far-field effects are important.

In the numerical study performed to derive the approximation formulas, the far-field exposure was represented by plane waves in the frequency range from 100 MHz to 5.5 GHz. The near-to-far field exposure was studied by numerical models of a femtocell and a WiFi access point (i.e. router and wireless modem) in the frequency range 1900–2500 MHz. The near-field exposure was simulated as a collection of different RF systems: (a) on-body RF devices; (b) specific RF devices (i.e. tablets, body-worn sensors, smartwatches, and VR devices); (c) laptop devices; and (d) portable devices, i.e. mobile and DECT phones over the frequency range from 800 MHz to 5.5 GHz. The exposure to mobile and DECT phones was already analyzed within the INTERPHONE (European Community Fifth Framework Programme (QLK4-CT-1999901563) and MOBI-Kids projects (European Community Seventh Framework Programme (Fp7/2007–2013, GA 226873)). Details about the analytical methods derived to evaluate the SAR induced by these RF systems can be found in^(9,23,24).

Figure 1 shows the exposure scenarios used to assess far-field, near-to-far field and near-field exposures. Far-field and near-field exposures were numerically assessed by solving the electromagnetic problem with the finite-difference time-domain (FDTD) method⁽²⁵⁾ implemented in the simulation platforms SEMCAD X64 Version 14.8 (Schmid and Partner Engineering, SPEAG, Switzerland) and Sim4Life Version 3.0 (ZMT Zurich MedTech, Switzerland), whereas FDTD software developed in-house was used for estimations of near-to-far field exposures^(26,27).

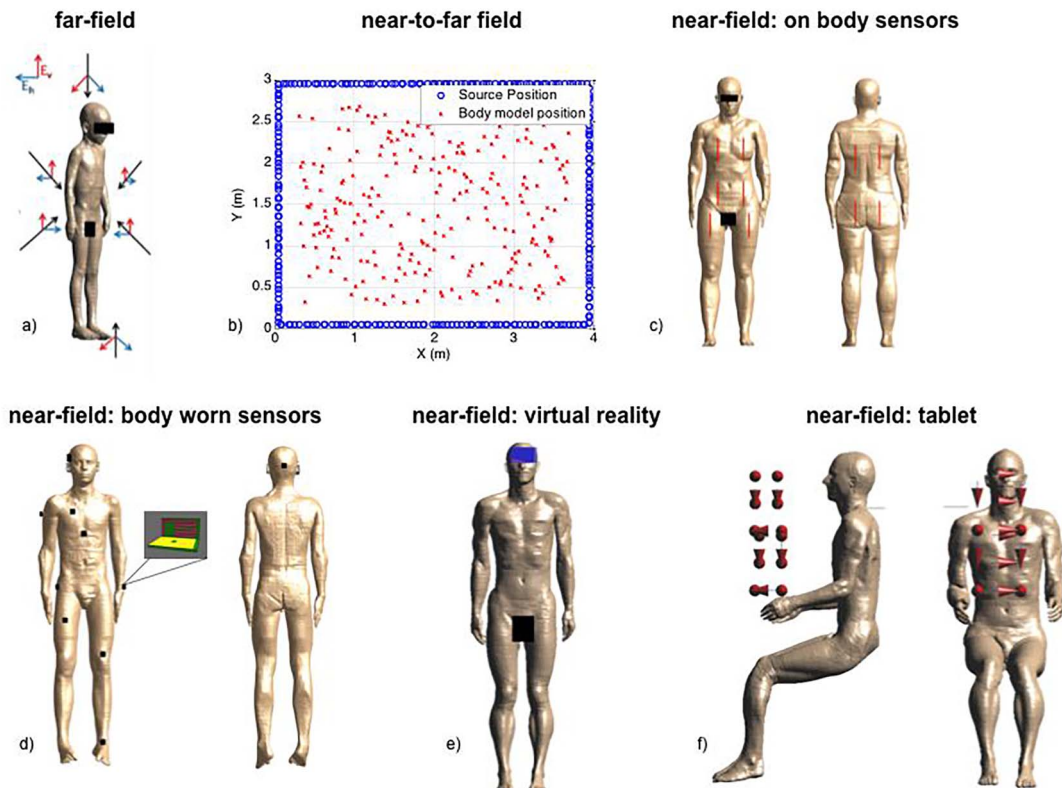


Figure 1: Examples of exposure scenarios analyzed to build the SAR approximation formulas. (a) Far-field exposure of the ViP phantom Billie (black arrows: incident field directions; red and blue arrows: potential E-field vectors); (b) potential positions of the RF systems (blue circles) and the exposed ViP phantom Eartha (red stars) in the near-to-far field exposure context. Near-field exposures to: (c) on-body sensors (represented as dipoles); (d) body-worn sensors on the ViP phantom Louis (locations are shown as dots, whereas the inset shows the antenna type used for all body-worn sensors); (e) wireless VR glasses (with integrated mobile phone) placed in front of Duke's eyes; and (f) a tablet/laptop/game console close to the ViP phantom Duke placed in a sitting posture. The potential antenna locations and orientations are shown as arrows.

Estimation of induced averaged SAR

In all exposure scenarios, the SAR_{wb} and SAR_{osa} ⁽³⁾ were calculated as:

$$SAR_{wb} = \frac{P_{abs_body}}{M_{body}} = \frac{1}{M_{body}} \int_{body} \sigma(r) E_{rms}(r)^2 dV \quad (1)$$

$$SAR_{osa} = \frac{P_{abs_organ}}{M_{organ}} = \frac{1}{M_{organ}} \int_{organ} \sigma(r) E_{rms}(r)^2 dV \quad (2)$$

where P_{abs_body} and P_{abs_organ} are the absorbed power in the whole body and the organ or tissue, respectively and, M_{body} and M_{organ} are the masses of the entire body and of each specific organ or tissue, σ is the conductivity, E_{rms} is the root mean square of the

induced E-field, and V is the volume. A particular SAR_{osa} that is investigated in multiple scenarios is the whole-brain averaged SAR, denoted SAR_{brain} , which takes into account RF-EMF absorption in all brain tissues.

For those exposure scenarios in which the RF device could be placed close to the head, the SAR_{osa} was also evaluated in each brain structure (SAR_{bs}) separately, through the Talairach Atlas tool implemented in SEMCAD X according to the method described in⁽²⁸⁾. This tool permits the induced SAR values achieved by the EMF simulation to be filtered by assigning each voxel of the numerical simulation to different brain levels (hemisphere level, structure level, gyrus level and cell level) according to the Talairach mapping of the brain. The SAR_{bs} is then calculated for different brain structures (i.e. frontal, temporal, parietal, occipital, limbic and

sublobar) as:

$$\text{SAR}_{\text{bs}} = \frac{P_{\text{abs,bs}}}{M_{\text{bs}}} = \frac{1}{M_{\text{bs}}} \int_{\text{bl}} \sigma(r) E_{\text{rms}}(r)^2 dV \quad (3)$$

where $P_{\text{abs,bs}}$ is the RF power absorbed by the brain structure and M_{bs} is the mass of the structure.

Approximation formulas in each exposure scenario

The approximation formulas derived in this study are derived for a set of input parameters. They can then be used to scale the SAR values in each specific exposure scenario by taking into account the characteristics of the exposed subject and of the RF system. The parameters that have an effect on the induced SAR might be different for each exposure scenario. Therefore, this study presents a set of formulas rather than a unique approximation formula. A detailed explanation about those approximation formulas that were developed in each exposure scenario is provided in the following subsections.

Far-field exposure

The goal of the far-field approximation formula was to estimate the induced SAR from measurements of the incident electric fields (E_{meas}) generated by the RF system under test. The approximation formula depends on several input parameters, which were classified as (a) fixed input parameters and (b) variable input parameters. The fixed input parameters for the far-field approximation formula consist of an SAR matrix resulting from FDTD simulations of ViP phantoms exposed to reference incident field strength E_{ref} . The variable input parameters consist in both the characteristics of the real subject, i.e. age, gender and body mass index (BMI), and in the incident E-field that was measured in a real exposure scenario (E_{meas}).

Far-field exposure was analyzed in six ViP phantoms (Table 1). The ViP phantoms were classified according to gender and age. This classification was used to relate the exposure of the phantom to that of a real subject through the variable input parameters of the approximation formula. The exposure was assessed by means of plane-wave-simulations at 10 frequencies between 50 MHz and 5.8 GHz (Table S1). The simulations for four out of six phantoms (Duke, Ella, Billie and Thelonus) were obtained from Djafarzadeh *et al.* (29). The field was incident from all six sides in two mutually orthogonal polarizations (Figure 1a), according to Djafarzadeh *et al.* (29). Simulations were executed at the same 10 frequencies using the same simulation set up as used in Djafarzadeh *et al.* (29) for the Charlie and Nina phantoms. Five SAR_{osa} values

(see Table 1) and a SAR_{wb} value were extracted from the numerical simulations. These were then averaged (over 12 incident plane waves) and interpolated to the central frequency of each frequency band listed in Table 2 to generate a matrix of $6 \times 16 \times 6$ (ViP phantoms \times frequency bands \times volumes/regions) SAR_{osa} values normalized to a reference incident E-field (E_{ref}) of 2.5 V/m. These values can be rescaled to any other incident E-field value at the same frequency (E_{meas}) using a factor $E_{\text{meas}}^2/E_{\text{ref}}^2$. The SAR approximation formula for far-field exposures translates the measured incident E-field (in V/m) into SAR values (in W/kg). The approximation consists of two steps: first, the human anatomical phantom most suitable as representative of the real subject in the numerical simulations for exposure to E_{ref} is chosen; then, all SAR values are normalized to E_{meas} :

$$\text{SAR}_{\text{osa}}(f) = \left(\frac{E_{\text{meas}}}{E_{\text{ref}}} \right)^2 \bullet \text{SAR}_{\text{osa,FDTD}}(f) \quad (4)$$

where $\text{SAR}_{\text{osa,FDTD}}$ is the interpolated SAR data obtained from the FDTD simulations using one of the six ViP phantoms and f is the frequency.

The SAR_{wb} is obtained by using the same normalization to E_{meas} and an additional normalization to the BMI of the subject (bmi):

$$\text{SAR}_{\text{wb}}(f) = \left(\frac{E_{\text{meas}}}{E_{\text{ref}}} \right)^2 \bullet \frac{bmi_{\text{model}}}{bmi} \bullet \text{SAR}_{\text{wb,FDTD}}(f) \quad (5)$$

where bmi_{model} is the BMI of the human anatomical model.

The approximation formula derived to predict the induced SAR in real exposure subject has uncertainties. The uncertainty on the fixed input parameters consists of two components. The first one is the simulation uncertainty on the individual plane wave simulations (e.g. grid resolution, dielectric properties, source model, boundary conditions), which can be obtained from literature such as Vermeeren *et al.* (30). The second component is the uncertainty on the angle of incidence and polarization of the exposure. This uncertainty is quantified as the variation of the SAR values (SAR_{osa} and SAR_{wb}) over the 12 incident plane waves at each simulated frequency.

The uncertainties on the variable input parameters can be estimated separately as: (a) uncertainty of the age ($u_{\text{mis,age}}$), which is a misclassification error related to the human anatomical phantom chosen and for which a worst-case estimate has been made by looking at the relative differences between the SAR induced in different phantoms of the same gender

at a given frequency; (b) uncertainty of the gender ($u_{\text{mis,gen}}$), which is a misclassification error estimated as the relative difference between the corresponding SAR values for different genders; (c) uncertainty in the BMI (u_{bmi}), which leads to a multiplicative uncertainty in the whole-body SAR but does not influence the uncertainty of the other OSAR values; and (d) uncertainty in the E_{meas} generated by the RF system (u_{source}), which depends heavily on the method of measurement.

Near-to-far field exposure

To build a SAR approximation formula for near-to-far field sources, an indoor exposure scenario in which the ViP phantom Eartha (see Table 1) exposed to an isotropic WLAN system at 2400 MHz was analyzed. Eartha was located at different positions inside a room with area $3 \times 4 \text{ m}^2$. The RF system was randomly placed near the wall at different heights (0.25 m–2 m) (Figure 1b). The radiation pattern of the WLAN system was measured with a system by Microwave Vision Group. The equivalence principle and spherical wave expansion were then used to simulate the source^(31–33). Details about this study can be found in Chiaramello *et al.*⁽³⁴⁾ and Wiart *et al.*^(26,27).

The approximation formulas for SAR_{wb} and SAR_{osa} were built on the basis of the polynomial chaos expansion (PCE)⁽³⁴⁾ and the low rank approximation⁽³⁵⁾. These approaches have already been cited in the literature in regards to surrogate models of exposure to EMFs^(34,36,37). With the PCE, the transfer approximation can be expressed as:

$$Y = M(X) = \sum_0^{P-1} \beta_\alpha \psi_\alpha(X) + \varepsilon = Y + \varepsilon \quad (6)$$

where X is a vector of input parameters on which the exposure depends, β_α are the unknown coefficients of the expansion, which need to be optimized, $\psi_\alpha(X)$ are the multivariate polynomials of degree α belonging to a polynomial basis $\Psi(X)$, and ε is the error of truncation. Section 3 of the supplementary materials provides more information on the form of the polynomials.

In this specific case, the vector X is composed of five uniformly-distributed input parameters: (a) the horizontal system position on the wall (distance traveled in clockwise direction along the blue line in Figure 1b) in the range [0.1:13.59] m; (b) the height of the system on the wall w.r.t. the floor in the range [0.25;2] m; (c) the position of the human in the room in the X-direction: [0.55: 3.45] m (Figure 1b) and (d) in the range [0.55: 2.45] m along the Y axis (Figure 1b); (e) the rotation of the human body around its main axis in the range [0.1;359] degrees.

The output vector Y , see Eq. 4, is either the SAR_{wb} or the SAR_{osa} . The SAR_{osa} is in this case only evaluated as an average over the whole brain, see Table 1.

Uncertainty evaluations were performed using numerical simulations in terms of the variability of both the system and position of the subject within the room, see Chiaramello *et al.*⁽³⁴⁾. Validation simulations for a specific set of configurations were executed and the SAR values obtained from those simulations were compared to those obtained by the approximation formulas.

Near-field exposure

Near-field exposures were analyzed in up to four ViP phantoms (Table 1). All RF systems were located at distances from the phantoms of $R < 0.62 \sqrt{\frac{D^3}{\lambda}}$. The RF systems considered in this study to represent a near-field exposure scenario were modeled as simplified generic antennas (Table 3). The near-Field exposure scenarios are divided in the following categories:

Near and on body sources provide localized exposure of the tissues with the region of exposure getting smaller and more intense with increasing proximity. This is illustrated in Figure 2a where a $\lambda/4$ dipole antenna is placed at a distance < 1 cm to the skin. Devices could be as close as or closer than 5 mm from the skin. Though devices might be placed close to almost any part of the body, 10 different locations close to the body representing five typical carrying positions of the mobile devices were identified as most common, namely: in the trouser pocket (back and front), in the jacket pocket (close to the chest and abdomen) and in a backpack (Figure 1c). The challenge in determining exposure to devices close to the body is to estimate the average tissue and organ exposure when the exact location of the source is not known and/or varies substantially with time. To address this, the following approach was taken, larger areas of the torso of a number of anatomical models where exposed using $\lambda/2$ dipole antennas further away (at 10 cm) from the body, see Figure 2b, relating to the 10 locations outlined above. The exposed regions from devices < 1 cm from the body and 10 cm from the body differ greatly (Figure 2a and b) however the relative exposure of tissues immediately below the device when normalized to the peak local SAR remains very similar, see Figure 2c. Hence the exposure of different tissues and organs (SAR_{osa}) by the $\lambda/2$ dipole is equivalent to an ‘average’ exposure as would be given by time averaging a multitude of device positions in closer proximity to the body. The remaining issue is how to normalize the magnitude of the exposure. Here we used the results available from the SEAWIND Project (‘Sound exposure and risk assessment of wireless network devices’, EU Fp7, GA 244149), which performed a large number of

Table 3. Overview of near-field RF system, frequencies, antenna type and body positions analyzed in this study. For all RF systems, the output power has been normalized to 1 W.

Near-field RF source	Frequency (MHz)	Generic antenna	Location at the body
Near and on body	866, 2000, 3500	$\lambda/2$ dipole antenna at 10 cm from body (Figure 1c)	-Trouser pocket (back and front) -Jacket pocket (close to the breast and to the womb) -In a backpack
Body-worn RF source	2450	Monopole antenna (Figure 1d)	Head, torso and legs
Smartwatch	2450	Monopole antenna (Figure 1d)	Left wrist
Wireless VR	866, 1900, 2450, 5500	$\lambda/4$ monopole antenna (Figure 1e)	Eyes
Tablet, laptop and phone in data mode	2450	$\lambda/2$ dipole antenna (Figure 1f)	<20 and >-30 cm distance from eyes and torso

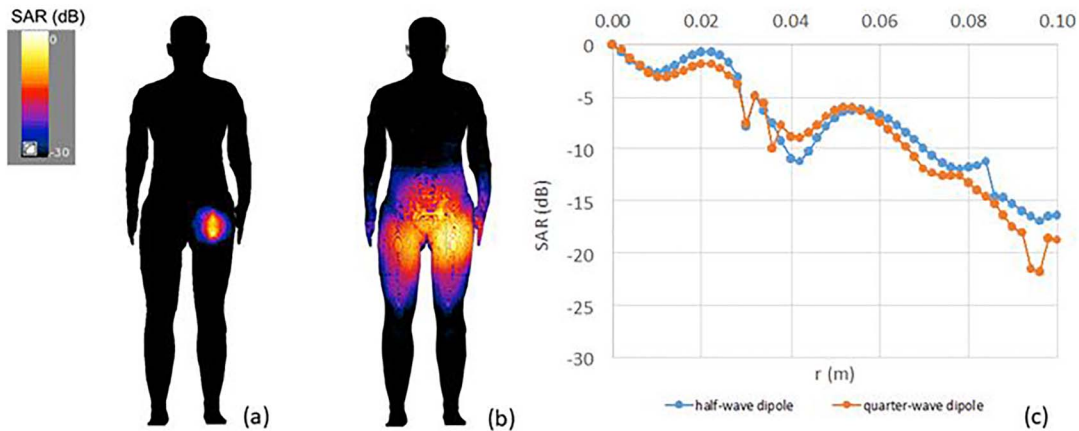


Figure 2: Example of SAR distribution on the surface of a human anatomical model. Frontal planar projection of SAR on the skin generated by: (a) $\lambda/4$ dipole antenna placed at 5 mm distance from the human body (SEAWIND Project), (b) $\lambda/2$ dipole antenna at the same frequency placed at 10 cm distance from the human body. Normalization is not to the same maximum SAR value, but to the maximum in each simulation. (c) Is the normalized SAR decay within the human body for $\lambda/4$ and $\lambda/2$ dipole antennas exposure at 866 MHz. The SAR is normalized to the value at the phantoms surface. r is the radial distance measured inside the body, measured from the skin on (0 m) in the direction perpendicular to the tangential plane to the skin.

simulations using $\lambda/4$ dipole antennas placed a few millimeters (5–9 mm) from the body. These results were used to normalize the averaged SAR_{wb} between $\lambda/2$ ('averaged exposures') and $\lambda/4$ dipole local exposures. The $\lambda/4$ dipole exposures were stated to provide a good approximation to the exposure from a typical mobile device antenna.

A generic wireless VR device was modeled according to the size of the commercially available VR Google Cardboard (<https://vr.google.com/cardboard/>), with a generic mobile phone placed in front of the VR device and modeled as a $\lambda/4$ inverted F antenna connected to a metallic ground enclosed in

a plastic case. The VR device model was always kept in front of the eyes but the monopole antenna was placed at different locations within the mobile phone (Figure 1e).

Body-worn sensors were modeled as meandered monopole antennas at 2450 MHz and placed at different locations close to the body (Figure 1d, Table 1).

Tablet and laptop devices were represented as $\lambda/2$ dipole antennas (arrows in Figure 1f) and placed at different locations and distances from the eyes and torso and with various possible locations of the antenna within the RF system considered.

For each RF system the average SAR values across different locations were calculated for each ViP model. A 3D-interpolation of the averaged SAR values was then estimated as a function of the frequency and the body mass through nonlinear least-squares optimization. The best SAR approximation formulas were found by minimizing the interpolation error of the average SAR values across all simulated positions as a function of the frequency and the body mass. Since the induced SAR values in a given tissue could vary substantially as a function of exact device location this represents the largest parameter of uncertainty for all near-field sources within any given epidemiological study. For this reason an approximation formula to predict the SAR variation due to the system location was generated, interpolating the standard deviation of the SAR value across different locations for each RF system.

Integrative exposure

In order to evaluate the potential total exposure of multiple RF systems, the sources are assumed to be incoherent for integration of the exposure and, therefore, the SAR values can be summed up after multiplication by their usage duration to obtain an integrated dose D_{int} in (J/kg). The D_{int} provides information about the total exposure of a subject, accounting for the contribution of all RF devices to which the subject is exposed and weighted with respect to both the exposure condition and duration in terms of position, type of use and frequency, as well as the estimated average output power of each device during normal usage. Specifically, the integrative exposure calculation consists of four main steps: (a) the (normalized) SAR values (W/kg/W) are estimated by the approximation formulas derived from each exposure scenario and each RF system; (b) the SAR values are scaled with respect to the actual output power (in W) of each specific RF system; (c) the SAR values are then scaled with respect to the time of use (minutes or min/day) of each RF system by each real exposed subject, through the data collected in epidemiological surveys. Dose values (J/kg) are therefore obtained for each specific RF system; (d) the dose values are summed up to obtain the integrative exposure in the entire body and/or in each tissue:

$$D_{int} = \sum_{source} \left(SAR \left(\frac{W}{kg} \right) \times \frac{Actual\ Output\ power\ (W)}{Simulated\ Output\ power\ (W)} \times Duration \left(\frac{min}{day} \right) \right) \quad (7)$$

Note that D_{int} can be a whole-body averaged value or an organ-specific value. In order to illustrate the use of our integrated RF-EMF exposure approach, we have applied it to a specific example of exposure of a female subject of 25 years old 169 cm in height and 67.7 kg in mass. The subject is exposed to far-field RF-EMFs of 1 V/m and a near-to-far field WiFi

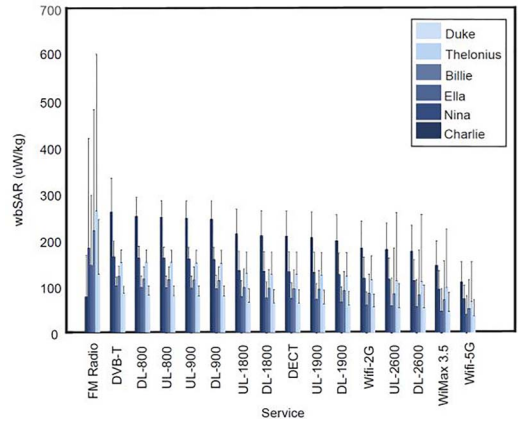


Figure 3: SAR_{wb} values under far-field exposure at 2.45 V/m. The bars indicate the average over 12 plane waves per phantom studied, whereas the whiskers indicate the average standard deviations. The different colors indicated the six different phantoms listed in Table 1. The bars are grouped according to those RF-frequency bands listed in Table 2.

access point during the whole day (24 h/day). The subject uses a laptop for 8 h, a tablet for 1 h, has another RF source such as a smartphone on or near the body for 1 h, uses a VR set for 0.5 h, and uses her phone to browse data via WiFi for 1 hour. All sources were assumed to emit 20 dBm (0.1 W) on average during the hour of usage, except the WiFi access point, which emitted 1 W of RF EMF power.

RESULTS

For all approximation formulas presented in this paper, the results of the numerical simulations relative to the far-field exposure scenario as well as the resulting coefficients of each approximation formula have been documented in the Supplementary Materials in Tables S2–S13.

Far-field exposure

Figure 3 shows the simulated SAR_{wb} values across different ViP phantoms over the 12 exposure scenarios analyzed in each frequency band listed in Table 2. Table S2 lists the average SAR_{wb} and whole-brain averages SAR_{osa} values as function of simulated frequency. The SAR_{wb} values generally decrease with increasing frequency. This can be explained as follows. The phantom with the highest mass (Duke) shows its maximal average SAR_{wb} (120 μ W/kg) for a fixed incident field strength (2.5 V/m) at the lowest studied frequency of 50 MHz. The phantom with the lowest mass (Charlie) shows a maximal average SAR_{wb} (22 μ W/kg) at 450 MHz for an incident field

strength of 2.5 V/m. The other phantoms studied under far-field exposure show maxima at frequencies in between 50 MHz and 450 MHz, see Figure 3. This frequency behavior is in line with what has been demonstrated in Bakker *et al.*⁽¹⁾. The frequency behavior is significantly different for the whole-brain averaged SAR, see Table S2. Here all phantoms except Nina show a maximum at 835 MHz. Nina shows a maximal SAR_{brain} at 450 MHz. Lauer *et al.*⁽¹⁷⁾ found maxima of SAR_{osa} for gray and white matter of the brain at 650 MHz and 900 MHz, respectively, which is very much in line with our results. The study of far-field exposure is important because subjects are potentially continuously exposed to such fields.

The combined, standard simulation uncertainty for fixed input parameters of 27% for SAR_{wb} and 29% for SAR_{brain} and SAR_{osa} was obtained from Bakker *et al.*⁽¹⁾.

The variable input parameters—the uncertainties u_{bmi} and u_{source} —are relative to the BMI and the incident E-field strengths, respectively, and depend on data coming from the real subjects and from measurements of the E-field. Section 2 of the supplementary materials (Tables S3 and S4) provides details on the analysis of the uncertainties associated with the variable input parameters. Fifty-one cases of potential misclassification based on gender and age of a subject were identified. In each of these cases, $u_{mis,age}$ and $u_{mis,gen}$ were quantified as the maximum relative deviation between the potential SAR value that could be assigned to the subject and that actually assigned to the subject.

Near-to-far field exposure

Supplementary Materials Tables S5 and S6 list the coefficients β_α of the polynomial expansion shown in Eq. 6, for prediction of SAR_{wb} and SAR_{brain}. It was found that the mean, median and maximum SAR_{wb} values were 0.13, 0.07 and 1.40 mW/kg, respectively, for an emitted power of 1 W. The corresponding SAR_{osa} values in the brain were 0.06, 0.03 and 3.7 mW/kg, respectively, for an emitted power of 1 W. A validation study of this approach was executed in Chiamarello *et al.*⁽³⁴⁾. They found error terms <11% on the prediction of SAR_{wb} and SAR_{brain} values. A similar study Pinto *et al.*⁽³⁸⁾ found mean and median SAR_{wb} values in a limited version of the same setup and for the same subject of 0.06 mW/kg and 0.05 mW/kg, respectively. These are close but slightly lower than what was found in this study.

Near-field exposure

Near- and on-body RF systems

When considering a possible function to fit both whole body and SAR_{osa} for the multitude of sim-

ulation results for both device operating frequency and the mass of the body, for devices with ill-defined placement with respect to the body, we are presented with a significant challenge. However, it is true that a small difference in frequency or body mass cannot physically result in a sudden change in SAR and resulting changes will be smooth. Some characteristics of the function can be anticipated. Organs deep within the body see reducing SAR with frequency as higher frequencies have smaller penetration depths, whereas superficial tissues see SAR increasing with frequency as energy is absorbed within a smaller volume closer to the surface. Tissues at intermediate depths can see an initial increase in SAR with frequency and then a reduction. All these features can be approximated by portions of a scaled sinusoidal function and reasonable fits for all tissues of interest can be achieved. One proviso is that where a given tissue or organ is far from the radiating device and exposure levels are low, the variation of SAR can become unpredictable and the uncertainty of the fit increases with the overall uncertainty of the actual exposure. The added uncertainty of the fitting function is always much less than the exposure uncertainty due to positioning uncertainty.

The sinusoidal SAR approximation formula parameters were optimized using a nonlinear least-square optimization for on-body RF devices. This formula can be used to estimate both SAR_{osa} in each specific tissue and SAR_{wb} (dB(W/kg)/W) as:

$$\begin{aligned} \text{SAR} = & \text{SAR}_{\text{off}} + \text{SAR}_f \times \cos\left(\left(\frac{f - f_0}{12000 \cdot c_1}\right) \times 2\pi\right) \\ & + \text{SAR}_m \times \cos\left(\left(\frac{\text{body_mass} - m_0}{1000 \cdot c_2}\right) \times 2\pi\right) \end{aligned} \quad (8)$$

where SAR_{off} (dBW/kg), SAR_f (dBW/kg), SAR_m (dBW/kg), f_0 (MHz) and m_0 (kg) are the optimized coefficients shown in the Supplementary Materials Table S7 (column from 2 to 6), $c_1 = 1$ MHz and $c_2 = 1$ kg. The constants in the expressions were chosen such that shape of the curves could be modeled for all tissues and the f_0 and m_0 parameter values allow curves of differing shapes to be fitted, i.e. increasing, decreasing, peaking etc. Specifically the magnitude of the variations in SAR are a function of SAR_f for the SAR expressed as a function of frequency in a subject of mass m , SAR_m for the SAR expressed as a function of the mass at a specific frequency f , whereas SAR_{off} adjusts the absolute value of the SAR prediction. Frequency f (MHz) and body_mass (kg) are the RF system operational frequency and the body mass of the real subject, respectively. The validity of the approximation is $20 \text{ kg} \leq \text{body_mass} \leq 120 \text{ kg}$ over the frequency

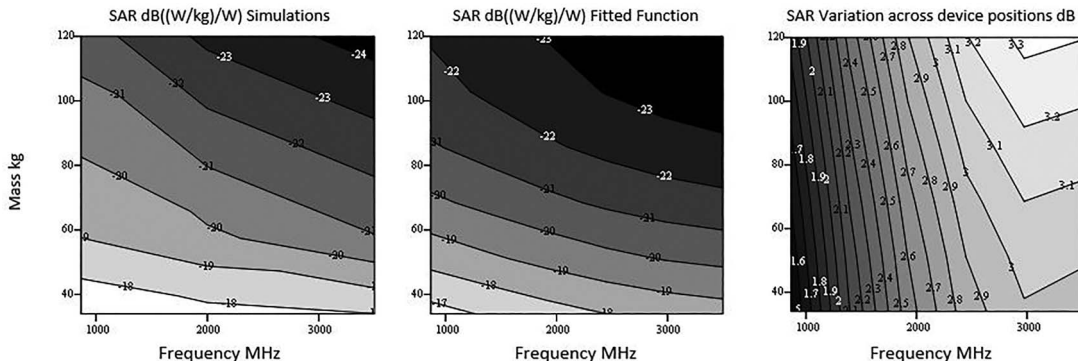


Figure 4: Normalized SAR_{wb} (W/kg/W) of the near and on-body devices expressed in dB ((W/kg)/W). Data from the numerical simulations (left) and fitted transfer approximation (middle) as a function of the frequency (MHz) and the body mass (kg) and the variation across possible device locations of the near and on-body device close to the body in dB (right).

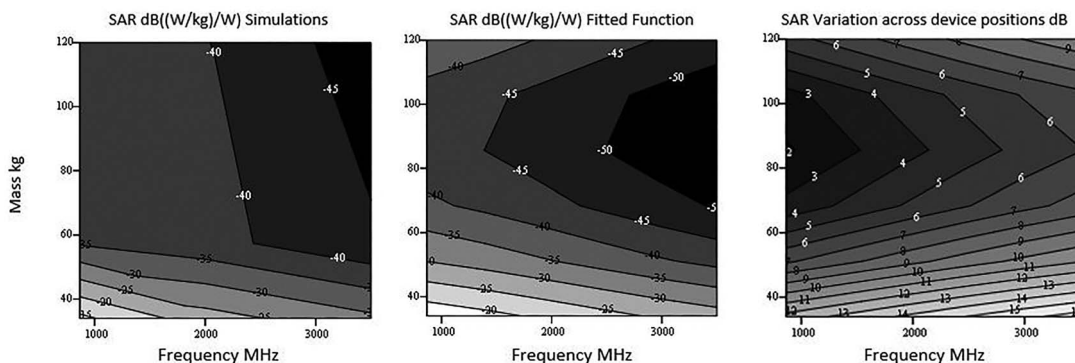


Figure 5: Whole-brain averaged SAR_{brain} in dB((W/kg)/W) induced by near and on-body devices. Data from simulations (left) and fitted transfer approximation (middle) as a function of the frequency (MHz) and the body mass (kg) and the variation across possible device locations close to the body in dB (right).

range $50 \text{ MHz} \leq f \leq 3.5 \text{ GHz}$. Outside this range the functions will become increasing erroneous.

The analysis of variations in the SAR values due to the RF system position with respect to the human body requires the estimation of the deviation around the average SAR values. Since the SAR_{wb} and SAR_{osa} are lognormally distributed, the variation of the SAR is expressed as the standard deviation of SAR values in dB across all system positions. The transfer function of the SAR variation used for both SAR_{wb} and SAR_{osa} is:

$$\begin{aligned} \text{variation} = & vSAR_{\text{off}} + vSAR_f \times \cos\left(\left(\frac{(f - v f_0)}{24000 \bullet c_1}\right)\right) \\ & \times 2\pi) + vSAR_m \times \cos\left(\left(\frac{(\text{body_mass} - vm_0)}{500 \bullet c_2}\right) \times 2\pi\right) \end{aligned} \quad (9)$$

where $vSAR_{\text{off}}$ (dB), $vSAR_f$ (dB), $vSAR_m$ (dB), $v f_0$ (MHz) and vm_0 (kg) are the coefficients optimized for

each SAR_{osa} and SAR_{wb} (as shown in the Supplementary Materials Table S7, columns 7–11).

Figures 4 and 5 show examples of the comparison between the simulation results and the fitted approximate formulas for the SAR_{wb} and the SAR_{brain} for the on-body and near body case plus the variation across the simulated positions. A fitting error of 0.5 dB was found in the estimation of SAR_{wb}, which can be seen to be much smaller than the observed variation of 1.63.3 dB, whereas, for SAR_{brain} which is some 100 times smaller than the SAR_{wb}, the interpolation error was <2.7 dB whereas the variation was in the range 6–17 dB, hence the fitting errors have little impact on the overall exposure estimation uncertainty. Figure 6 shows, as an example, the SAR_{wb} values across a range of frequencies and exposed subjects of different masses estimated through the approximation formula (8) and adjusted with respect to the interpolation error (in Figure 6 the middle of the box is the calculated value through the formula (8) and the lower

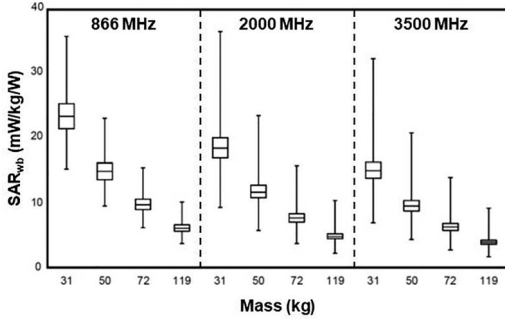


Figure 6: Near- and on-body RF systems: example of SAR_{wb} calculated for four body masses at the frequencies of 866, 2000 and 3500 MHz. The body mass is indicated on the horizontal axis. The central line in each box represents the SAR_{wb} estimated from the approximation formula (8), the upper and lower bounds of the box include the fitting error, whereas the whiskers indicate the SAR_{wb} variation due to the location of the RF device at the human body estimated from formula (9) for an input power of 1 W.

and upper level of the box represent the interpolation error). The SAR variation estimated through the approximation formula (9) accounts also for the variability in the position of the RF system and is represented by the whiskers in Figure 6. In general terms, the exposure tends to decrease with increasing frequency and body mass.

Body-worn sensors

SAR approximation formulas for body-worn sensors were built as a function of the masses at the frequency of 2450 MHz. In analogy with the previously found approximation formula for near and on-body RF systems the SAR approximation formula can be expressed as:

$$SAR = SAR_{off} + SAR_m \times \cos\left(\left(\frac{(body_mass - m_0)}{400 \bullet c_2}\right) \times 2\pi\right) \quad (10)$$

where SAR_{off} (dBW/kg), SAR_m (dBW/kg), and m_0 (kg) have been optimized for each SAR_{osa} and SAR_{wb} separately (the optimized coefficients are shown in the Supplementary Materials in Table S8–S10, columns 2–4). The approximation formula for estimation of SAR induced by body-worn sensors is applicable over the range $20 \text{ kg} \leq body_mass \leq 120 \text{ kg}$ at 2450 MHz.

For all approximation formulas used to estimate the SAR_{wb} and SAR_{osa} the error of interpolation was always found to be $< 2\%$.

The variation of SAR_{osa} and SAR_{wb} due to the uncertainty in the location of body-worn sensor in each specific region was calculated as well and can be

expressed with the following formula:

$$\begin{aligned} \text{variation} &= vSAR_{off} + vSAR_m \\ &\times \cos\left(\left(\frac{(body_mass - vm_0)}{400 \bullet c_2}\right) \times 2\pi\right) \quad (11) \end{aligned}$$

the optimized coefficient $vSAR_{off}$ (dB), $vSAR_m$ (dB) and vm_0 (kg) for SAR_{wb} and SAR_{osa} variation are reported in the Supplementary Materials on Table S8–S10, columns 5–7.

Wireless VR device

An approximation formula similar to (8) has been built to estimate SAR_{brain} and SAR_{wb} , whereas for SAR_{bs} , the following equation is used:

$$\begin{aligned} SAR_{bs} &= SAR_{off} + SAR_f \times \cos\left(\left(\frac{(f - f_0)}{15000 \bullet c_1}\right) * 2\pi\right) \\ &+ SAR_m \times \cos\left(\left(\frac{(head_mass - m_0)}{50 \bullet c_2}\right) \times 2\pi\right) \quad (12) \end{aligned}$$

The optimized coefficients are shown in the Supplementary Materials in Table S11, columns 2–6. The approximation is applicable for head_mass up to 7 kg over the frequency range $50 \text{ MHz} \leq f \leq 6 \text{ GHz}$, which represents an upper boundary body mass of the average adult head. Though head mass is easy to determine for an anatomical model, the same cannot be said for the head of a person. However there is a good correlation between head mass/body mass and age in years that can be employed:

For age < 20 years $head_mass = body_mass \times 0.5063 \times age^{-0.638}$ otherwise $0.0747 \times body_mass$.

The fitting error of SAR_{wb} and SAR_{brain} was $< 10\%$, whereas in the SAR_{bs} the error tends to increase to $> 50\%$ due to the small size of the interested regions.

The variation of the exposure is assessed in terms of the uncertainty in the antenna location in the mobile phone, and the transfer approximation is similar to equation (8) (coefficients in the Supplementary Material, Table S11, columns 7–11).

Tablet, laptop or phone in data-use mode

Transfer approximations for each position of a tablet, laptop, or phone in data-use mode, similar to those used for body-worn sensor devices (Eqs. 10 and 11), were built as a function of the human body mass, and for the SAR_{bs} as a function of the head mass, on the basis of the averaged SAR values across the four locations of the dipole antenna for each tablet position. The variation of the exposure was assessed for each tablet position as uncertainty in the antenna location inside the device, according to transfer approximation

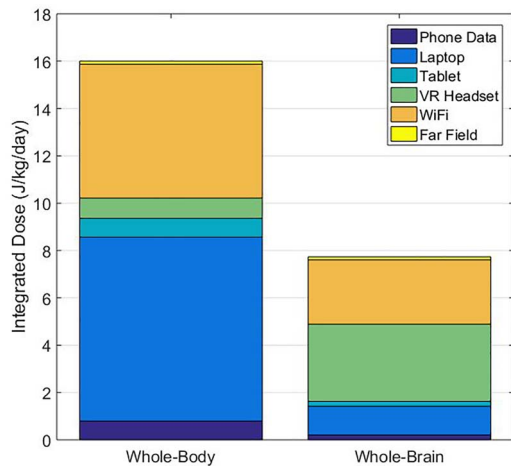


Figure 7: Example of integrative exposure expressed as daily dose (J/kg) of each RF system for the whole body and the whole brain in a real 25-year-old female subject with 169 cm whole-body height and 67.7 kg in mass. The subject is exposed to far-field RF-EMFs of 1 V/m and a near-to-far field WiFi access point during the whole day (24 h/day). The subject uses a laptop for 8 h, a tablet for 1 h, has another RF source such as a smartphone on or near the body for 1 hour, uses a VR set for 0.5 h, and uses her phone to browse data via WiFi for 1 h. All sources were assumed to emit 20 dBm (0.1 W) on average during the hour of usage, except the WiFi access point, which emitted 1 W of RF EMF power. The left bar shows the whole-body dose, whereas the right bar shows the brain-specific dose. Different segments of the bars (in different colors) indicate different RF-EMF sources.

similar to Eq. (11). Similar to the results obtained for the SAR transfer approximation of body-worn sensors, the fitting error was $\ll 2\%$. The optimized coefficients for use in Eqs. 10 and 11 are listed in the Supplementary Materials in Table S12, columns 2–4 and 5–7 for the SAR and variation, respectively.

Example of integrative exposure

Figure 7 shows an example of contributions to the daily dose of several RF systems in the whole body and in the whole brain of a 25-year-old female subject under the conditions described in the Section Materials and Methods. In this example, the subject is exposed to several RF systems simultaneously. The contribution of the far-field exposure was calculated by summing the contribution of all analyzed frequency bands described in the Section Materials and Methods. The relative contribution of each RF system is heavily dependent on the distance to the human body (for SAR_{wb}) and to the human head (for whole-brain SAR), respectively. We found a daily whole-body integrated dose of 16 J/kg/day and a daily whole-brain integrated dose of 7.7 J/kg/day in this

example. These values are much higher than the ones listed in Lauer *et al.*⁽¹⁷⁾, although we found very good agreement in SAR values. This can be explained by the scenarios considered in Lauer *et al.*⁽¹⁷⁾, where usage < 1 h per week of a mobile device was considered. Although in our example, we use multiple hours of exposure per day. The laptop and near-to-far field WiFi exposure is the dominant component that contributes to the SAR_{wb} . The WiFi access point is an RF-EMF exposure source that illuminates the whole body during a full day (in this example), whereas the laptop exposure is relatively high in terms of dose because of the 8 h of exposure in this example. Far-field RF-EMFs contribute very little to whole-body ($< 1\%$) and whole-brain (1.6%) dose. Note that some RF-EMF sources, such as laptop use, can have a significant contribution to the whole-body dose, because they are used close to the body and thus cause relatively high absorption of RF-EMFs in the body, but contribute far less to the whole-brain dose, see Figure 7. Integrated RF-EMF doses have previously been used to study longitudinal exposure to RF EMFs fields^(13,14), using specific integrated dose calculations tailored to those studies. This work provides a generally usable estimation method for integrated RF-EMF exposure that could be used in future studies.

CONCLUSIONS

In this study, an easy-to-use approach for fast estimation of RF-EMF exposure in terms of SAR within the human body resulting from simultaneously operated RF systems in different exposure scenarios is proposed. System-specific analytical approximation formulas for quantification of the absorbed power of several RF systems over a wide range of human subjects and frequencies, accounting for variations in system location, posture, age, sex and morphology were developed. To this aim, numerical simulations of advanced human anatomical phantoms exposed to several RF systems to simulate far-field, near-to-far field, and near-field exposure conditions were executed and analyzed. The approximation formulas permit to have an estimation of the absorbed power in the whole body, tissues and organs and different brain regions. Since the general population is normally exposed to numerous sources of RF exposure during the day, these approximation formulas represent a useful tool for epidemiology studies to predict the cumulative exposure for assessment of health impact. Indeed, the SAR levels can be combined with personal information about the conditions and duration of use of each RF source and scaled with respect to the actual output power of each device to obtain typical and personal integrated and cumulative RF doses.

ACKNOWLEDGEMENTS

We thank Niels Kuster and Sabine Regel (SR-Scientific GmbH) for critical review of the study and Patricia L. Bounds for copyediting the manuscript.

FUNDING

European Union's FP7 Programme within the framework of the international project GERONIMO ('Generalized EMF Research using Novel Methods—an integrated approach: from research to risk assessment and support to risk management', GA603794, 01/2014–12/2018); ANSES—Agence nationale de securite sanitaire de l'alimentation, de l'environnement et du travail within the Project CREST ('Characterization of exposure to radiofrequency (RF) induced by new uses and technologies of mobile communication systems', 2013–2017); Arno Thielens is a fellow supported by the European Union's Horizon 2020 Research and Innovation Programme under the Marie Skłodowska-Curie grant agreement No 665501 with the research foundation Flanders (FWO). Mònica Guxens is funded by a Miguel Servet fellowship (MS13/00054, CP13/00054, CPII18/00018) awarded by the Spanish Institute of Health Carlos III. We acknowledge support from the Spanish Ministry of Science and Innovation and the State Research Agency through the 'Centro de Excelencia Severo Ochoa 2019-2023' Program (CEX2018-000806-S), and support from the Generalitat de Catalunya through the CERCA Program.

REFERENCES

- Bakker, J. F., Paulides, M. M., Christ, A., Kuster, N. and van Rhooon, G. C. *Assessment of induced SAR in children exposed to electromagnetic plane waves between 10 MHz and 5.6 GHz*. *Phys. Med. Biol.* **55**, 3115–3130 (2010).
- Christ, A. *et al.* *The virtual family – development of surface-based anatomical models of two adults and two children for dosimetric simulations*. *Phys. Med. Biol.* **55**, N23–N38 (2010).
- Thielens, A., Vermeeren, G., Joseph, W. and Martens, L. *Stochastic method for determination of the organ-specific averaged SAR in realistic environments at 950 MHz*. *Bioelectromagnetics* **34**, 549–562 (2013).
- Dürrenberger, G., Fröhlich, J., Rössli, M. and Mattsson, M. O. *EMF monitoring-concepts, activities, gaps and options*. *Int. J. Environ. Res. Public Health* **11**, 9469–9479 (2014).
- Varsier, N., Plets, D., Corre, Y., Vermeeren, G., Joseph, W., Aerts, S., Martens, L. and Wiart, J. *A novel method to assess human population exposure induced by a wireless cellular network*. *Bioelectromagnetics* **36**, 451–463 (2015).
- International Agency for Research on Cancer (IARC). *Non-Ionizing Radiation, Part 2: Radiofrequency Electromagnetic Fields*. IARC Volume. (Lyon, France: IARC) p. 102 (2013).
- World Health Organization (WHO). *WHO Research Agenda for Radiofrequency Fields*. (Geneva, Switzerland: World Health Organization) (2010).
- Vrijheid, M. *et al.* *Determinants of mobile phone output power in a multinational study: implications for exposure assessment*. *Occup. Environ. Med.* **66**(10), 664–671 (2009).
- Cardis, E. *et al.* *Estimation of RF energy absorbed in the brain from mobile phones in the interphone study*. *Occup. Environ. Med.* **68**, 686–693 (2011). doi: 10.1136/oemed-2011-100065.
- Van Wel, L., Huss, A., Liorni, I., Capstick, M., Wiart, J., Joseph, W., Thielens, A., Cardis, E. and Vermeulen, R. *Organ-specific integrative exposure assessment: radio-frequency electromagnetic field exposure and the contribution of sources in the general population*. *Occup. Environ. Med.* **75**, A12 (2020).
- Hombach, V., Meier, K., Burkhardt, M., Kuhn, E. and Kuster, N. *The dependence of EM energy absorption upon human head modeling at 900 MHz*. *IEEE Trans. Microw. Theory Tech.* **44**(10), 1865–1873 (1996).
- Drossos, A., Santomaa, V. and Kuster, N. *The dependence of electromagnetic energy absorption upon human head tissue composition in the frequency range of 300–3000 MHz*. *IEEE Trans. Microw. Theory Tech.* **48**(11), 1988–1995 (2000).
- Schoeni, A., Roser, K. and Rössli, M. *Memory performance, wireless communication and exposure to radiofrequency electromagnetic fields: a prospective cohort study in adolescents*. *Environ. Int.* **85**, 343–351 (2015).
- Foerster, M., Thielens, A., Joseph, W., Eeftens, M. and Rössli, M. *A prospective cohort study of adolescents' memory performance and individual brain dose of microwave radiation from wireless communication*. *Environ. Health Perspect.* **126**(7), 077007 (2018).
- Cabrè-Riera, A. *et al.* *Estimated whole-brain and lobe-specific radiofrequency electromagnetic fields doses and brain volumes in preadolescents*. *Environ. Int.* **142**, 105808 (2020).
- Roser, K. *et al.* *Development of an RF-EMF exposure surrogate for epidemiologic research*. *Int. J. Environ. Res. Public Health* **12**(5), 5634–5656 (2015).
- Lauer, O., Frei, P., Gosselin, M. C., Joseph, W., Rössli, M. and Fröhlich, J. *Combining near- and far-field exposure for an organ-specific and whole-body RF-EMF proxy for epidemiological research: a reference case*. *Bioelectromagnetics* **34**, 366–374 (2013).
- Plets, D., Joseph, W., Aerts, S., Vanhecke, K., Vermeeren, G. and Martens, L. *Prediction and comparison of downlink electric-field and uplink localized SAR values for realistic indoor wireless planning*. *Radiat. Prot. Dosimetry* **162**, 487–498 (2013).
- Gosselin, M.-C. *et al.* *Development of a new generation of high-resolution anatomical models for medical device evaluation: the virtual population 3.0*. *Phys. Med. Biol.* **59**, 5287–5303 (2014).

20. Bhatt, C. R. R., Thielens, A., Billah, B., Redmayne, M., Abramson, M. J., Sim, M. R., Vermeulen, R., Martens, L., Joseph, W. and Benke, G. *Assessment of personal exposure from radiofrequency-electromagnetic fields in Australia and Belgium using on-body calibrated exposimeters*. Environ. Res. **151**, 547–563 (2016).
21. Baracca, P., Weber, A., Wild, T. and Grangeat, C. *A statistical approach for RF exposure compliance boundary assessment in massive MIMO systems*. In WSA 2018; 22nd International ITG Workshop on Smart Antennas, pp. 1–6. VDE, (2018).
22. Balanis, C. A. *Antenna Theory: Analysis and Design*. (John Wiley & sons) (2016).
23. Sadetzki, S. *et al. The MOBI-kids study protocol: challenges in assessing childhood and adolescent exposure to electromagnetic fields from wireless telecommunication technologies and possible association with brain tumor risk*. Front. Public Health **2**, 124 (2014).
24. Calderon, C. *et al. Estimation of ELF and RF Exposure in the Brain from Mobile Phones in the MOBI-Kids Study* (submitted). (2020).
25. Taflove, A. and Hagness, S. C. *Computational Electrodynamics. The Finite-Difference Time Domain Method*, third edn. (Boston MA USA: Artech House) (2005).
26. Wiart, J., Kersaudy, P., Pinto, Y., Mostarshedi, S. and Picon, O. Near field numerical dosimetry using spherical wave expansion and advanced statistical methods. In: Proceedings of URSI Asia-Pacific Radio Science Conference. (Seoul Korea) pp. 728–730 (2016, 2016).
27. Wiart, J. *Radio-Frequency Human Exposure Assessment: From Deterministic to Stochastic Methods*. (Hoboken NJ USA: John Wiley & Sons) (2016).
28. Crespo-Valero, P., Christopoulou, M., Zefferer, M., Christ, A., Achermann, P., Nikita, K. S. and Kuster, N. *Novel methodology to characterize electromagnetic exposure of the brain*. Phys. Med. Biol. **56**, 383–396 (2011).
29. Djafarzadeh R, Crespo-Valero P, Zefferer M, Kuehn S, Christ A, and Kuster N. 2009. Organ and CNS Tissue Region Specific Evaluation of the Time-Averaged Far-Field Exposure in Various Human Body Models. Joint Meeting of the Bioelectromagnetics Society and the European BioElectromagnetics Association, Davos, Switzerland, June 14–19.
30. Vermeeren, G., Joseph, W. and Martens, L. *Statistical multi-path exposure method for assessing the whole-body SAR in a heterogeneous human body model in a realistic environment*. Bioelectromagnetics **34**(3), 240–251 (2013).
31. Hansen, J. E. *Spherical Near-Field Antenna Measurements*. (London, UK: Peter Peregrinus on behalf of the Institution of Electrical Engineers) (1988).
32. Jensen, F., Frandsen, A. and Copenhagen, D. *On the number of modes in spherical wave expansions*. Proc. 26th Antenna Meas Tech Assoc Meet. Symp. **2**, 489–494 (2004).
33. Merewether, D., Fisher, R. and Smith, F. *On implementing a numeric Huygens source scheme in a finite difference program to illuminate scattering bodies*. IEEE Trans. Nucl. Sci. **27**, 1829–1833 (1980).
34. Chiaramello, E., Parazzini, M., Fiocchi, S., Ravazzani, P. and Wiart, J. *Stochastic dosimetry based on low rank tensor approximations for the assessment of children exposure to WLAN source*. IEEE J. Electromagn. RF Microw. Med. Biol. **2**, 131–137 (2018).
35. Chevreuril, M., Lebrun, R., Nouy, A. and Rai, P. *A least-squares method for sparse low rank approximation of multivariate functions*. SIAM/ASA J. Uncertain Quantif. **3**, 897–921 (2015).
36. Liorni, I., Parazzini, M., Fiocchi, S. and Ravazzani, P. *Study of the influence of the orientation of 50 Hz magnetic field on the fetal exposure using polynomial chaos decomposition*. Int. J. Environ. Res. Public Health **12**, 5934–5953 (2015).
37. Liorni, I., Parazzini, M., Varsier, N., Hadjem, A., Ravazzani, P. and Wiart, J. *Exposure assessment of one-year-old child to 3G tablet in uplink mode and to 3G femtocell in downlink mode using polynomial chaos decomposition*. Phys. Med. Biol. **61**, 3237–3257 (2016).
38. Pinto, Y. and Wiart, J. *Statistical analysis and surrogate modeling of indoor exposure induced from a WLAN source*. In: In 2017 11th European Conference on Antennas and Propagation (EUCAP) (pp. 806–810). (IEEE) (2017).